arXiv:2004.05234v1 [cs.CV] 10 Apr 2020

Attend and Decode: 4D fMRI Task State Decoding Using Attention Models

Sam Nguyen[1], **Brenda Ng, Alan Kaplan and Priyadip Ray**
Lawrence Livermore National Lab
7000 East Ave
Livermore, CA 94550
[1]nguyen116@llnl.gov

Abstract

Functional magnetic resonance imaging (fMRI) is a neuroimaging modality that captures the blood oxygen level in a subject's brain while the subject performs a variety of functional tasks under different conditions. Given fMRI data, the problem of inferring the task, known as *task state decoding*, is challenging due to the high dimensionality (hundreds of million sampling points per datum) and complex spatio-temporal blood flow patterns inherent in the data. In this work, we propose to tackle the fMRI task state decoding problem by casting it as a 4D spatio-temporal classification problem. We present a novel architecture called *Brain Attend and Decode* (BAnD), that uses residual convolutional neural networks for spatial feature extraction and self-attention mechanisms for temporal modeling. We achieve significant performance gain compared to previous works on a 7-task benchmark from the large-scale Human Connectome Project (HCP) dataset. We also investigate the transferability of BAnD's extracted features on unseen HCP tasks, either by freezing the spatial feature extraction layers and retraining the temporal model, or finetuning the entire model. The pre-trained features from BAnD are useful on similar tasks while finetuning them yields competitive results on unseen tasks/conditions.

Introduction

Functional MRI (fMRI) is a neuroimaging modality that measures spatial differences in blood oxygenation over time. As opposed to forming a static structural image of the brain, fMRI captures temporal activity patterns. A contrast mechanism is used to generate the Blood Oxygen Level Dependent (BOLD) signal which may be used to infer brain activities by measuring relative oxygen concentrations in the blood (Webb and Kagadis 2003). Active brain regions elicit greater concentrations of oxygenated blood, resulting in greater contrast in the fMRI images. The ability to record whole brain activity in a noninvasive manner makes fMRI an attractive option for studying brain function.

During the fMRI procedure, a subject lies on a MRI scanner, is subjected to a stimulus, then performs various tasks to activate different brain regions. The goal of fMRI task state decoding is to map the fMRI sequence to the task that was performed. The fMRI sequence is a movie of 3D volumes, that contains complex spatio-temporal patterns. Associating these patterns to the task is beneficial for (1) insight discovery into the inner workings of the brain, and (2) diagnosis of neurological disorders. Due to the availability of data and the non-invasive procedure, fMRI holds great promise for exploring the complex landscape of the human brain.

While many analytic techniques (Naselaris et al. 2011; Wen et al. 2018) have been developed for fMRI task state decoding, many challenges remain. Increasing resolution and growing acquisition rates of modern scanners as well as scarcity of subjects and spatio-temporal complexity of the blood oxygenation levels pose significant computational, memory problems. In this paper, we address these problems by taking temporal dynamics into account, and computing spatio-temporal maps to indicate relative importance of brain regions for the task decoding.

Our proposed model, called *Brain Attend and Decode* (BAnD), has been validated using the current state-of-the-art neuroimaging dataset from the Human Connectome Project (HCP) (Van Essen et al. 2013; Glasser et al. 2016). HCP contains multiple types of neuroimaging, demographic information, and cognitive scoring of over 1,000 healthy young adults (HCP-YA). For this work, we train and test our models on the task fMRI (tfMRI) data, which corresponds to fMRI data collected when the subject is tasked with cognitive tasks (reciting a story, guessing a number, etc.) while lying on the scanner. The cognitive tasks in HCP-YA involve Emotion, Language, Gambling, Motor, Relational, Social, and Working Memory (Barch et al. 2013).

Contributions:

- We propose the first attention-based model for processing 4D spatio-temporal data. Based on the multi-head self-attention model (Vaswani et al. 2017) and the pooling operation (Devlin et al. 2018), we develop a self-attention model that attends to a series of embedded 3D frames.
- Our model achieves substantial improvement in classification performance over previous works on task state decoding using the 7-task benchmark from the HCP dataset.
- We demonstrate transfer learning of the learned features under different conditions and tasks.
- We visualize the relative importance of brain regions and frames, with respect to task state decoding, by computing

spatial and temporal maps.

Related Work

Recently, there has been much interest in applying machine learning (ML) to fMRI data (Pereira, Mitchell, and Botvinick 2009). The approaches taken are either one of: (1) ML techniques using hand-crafted features, or (2) deep learning techniques which automatically extract features from the raw data. In general, especially for imaging applications, deep learning outperform traditional ML techniques based on hand-crafted features (Litjens et al. 2017).

In the context of image classification, convolutional neural networks (CNNs) have shown great success in extracting high-level concepts from raw pixel-valued images, so a reasonable approach would be to adopt CNNs to learn representational features from fMRI data. (Huang et al. 2017) proposed an architecture based on the sparse convolutional autoencoder to learn high-level features from handcrafted time series derived from the raw fMRI data. (Wang et al. 2018) proposed a 4-layer CNN that classifies tasks from the raw fMRI voxel values. Both works were demonstrated on HCP and the entire fMRI sequence is input into the model.

More recent efforts attempt to use sequence models to capture temporal correlations, so that the model would ingest each frame of the fMRI sequence as input. (Mao et al. 2019) used a CNN to extract features from each fMRI frame, then applied each frame's feature as input into a Long Short-Term Memory (LSTM) (Hochreiter and Schmidhuber 1997) model. Improved variants include: (Thomas et al. 2018) who used a bi-directional LSTM in conjunction with a CNN, and (Pominova et al. 2018) who used a LSTM in conjunction with a Residual network (ResNet) (He et al. 2016).

Unlike RNNs and LSTMs that process data sequentially and rely on short-term memory to make predictions, attention models simultaneously process all the data in the entire sequence, offering superior performance (Bahdanau, Cho, and Bengio 2014) and parallelizability. Attentions models are also more amenable to interpretation (Xu et al. 2015). Due to advantages offered by attention models, we present the first attention-based model for 4D fMRI data that incorporates the Transformer (a multi-headed self-attention module), and demonstrate its utility in fMRI task state decoding.

Preliminaries

In this section, we briefly review preliminary concepts.

Convolutional Neural Network (CNN): Originally developed for image classification (LeCun et al. 1998) and has since been extended to other modalities (text and audio), a CNN defines a mapping from an input 3D volume ($W \times H \times D$, where D is the number of channels for an image of size $W \times H$) to a scalar class score. A CNN is a neural network that generally comprises of repeated computational blocks of interleaving convolutional, pooling and activation layers. The convolutional layer detects patterns within a local receptive field in the input image (via dot products with a small, shared-weight filter), while the pooling layer downsamples by taking the average or the maximum value. The activation layer has the same function as in standard neural networks – to introduce nonlinearity into the model. The chaining of these computational blocks in a CNN allows it to learn hierarchical, translation-invariant features efficiently.

Residual Network (ResNet): A residual network is a CNN that has residual layers (He et al. 2016). A residual layer is akin to a shortcut connection between layers. Let $\mathcal{H}(\mathbf{x})$ denote the desired mapping to be learned. Instead of learning $\mathcal{H}(\mathbf{x})$ directly, a *residual* mapping $\mathcal{F}(\mathbf{x}) = \mathcal{F}(\mathbf{x}) - \mathbf{x}$ is learned by way of a residual layer. If the additional layer introduces no gain to the network, then the residual layer will simply learn the identity mapping. Thus, the signal would not be degraded despite the additional layer. Each residual function $\mathcal{F}$ is implemented as a bottleneck block, that effectively performs dimension reduction for faster training. These concepts have been instrumental to the successful training of very deep neural networks; many are now established benchmark CNNs for image feature extraction.

Long Short-Term Memory Networks (LSTMs): A LSTM (Hochreiter and Schmidhuber 1997) is a type of recurrent neural network (RNN) that takes in sequence inputs, and is designed to retain long-term dependencies within the sequence. It does so via three "gates", that control for selective forgetting of the cell state, remembering of the new input, and filtering of the updated cell state into an output. Like ResNet, a LSTM allows signals to bypass (via the gates) so it can retain information across longer time steps than a RNN.

Transformers: RNNs and LSTMs are limited in that they are constrained to process data sequentially. Transformers (Vaswani et al. 2017) offer a different way to reason about sequence data, by *not* treating them as sequence, but rather, processing the entire sequence of data all at once. It applies self-attention to the entire sequence to model relationships between the tokens in the sequence. These relationships are quantified as attention scores, which in turn determine how much each token would contribute the embedding of a given context token at the next layer. Specifically, the embedding of the context token is derived from a feed-forward neural network that takes as input the weighted average of all the tokens' embeddings, in which the attention scores are weights. Transformers have been gaining in popularity for sequence reasoning, due to their improved performance and parallelizability over RNNs. The attention scores can also be visualized to elucidate the flow of information (Devlin et al. 2018; Girdhar et al. 2018) within the model.

Methods

An instance of the fMRI data is a tuple $(\mathbf{x}_{1:T}, \mathbf{y})$, where $\mathbf{x}_{1:T} = \{\mathbf{x}_1, \mathbf{x}_2, ..., \mathbf{x}_T\}$ is a sequence of 3D frames and each frame $\mathbf{x}_t \in \mathbb{R}^3$ is a snapshot of the subject's brain activity at time t. $\mathbf{y}$ are the tasks and associated conditions under which $\mathbf{x}_{1:T}$ was captured during the fMRI procedure. Inferring $\mathbf{y}$ from $\mathbf{x}_{1:T}$ is known as fMRI task state decoding – a challenging problem due to the complex dynamics in both spatial and temporal dimensions. In this work, we seek to improve the state-of-the-art by using the Transformer to model temporal dynamics inherent in fMRI data. Due to the lack of code and data processing scripts from previous works, we reimplemented the baseline models and com-

Layer Name	**3D ResNet-18** (kernel size, number of filters, stride)
conv1	$7 \times 7 \times 7, 64$, stride 2
conv2	$\begin{bmatrix} 3 \times 3 \times 3, 64, 1 \\ 3 \times 3 \times 3, 64, 1 \end{bmatrix} \times 2$
conv3	$\begin{bmatrix} 3 \times 3 \times 3, 128, 2 \\ 3 \times 3 \times 3, 128, 2 \end{bmatrix} \times 2$
conv4	$\begin{bmatrix} 3 \times 3 \times 3, 256, 2 \\ 3 \times 3 \times 3, 256, 2 \end{bmatrix} \times 2$
conv5	$\begin{bmatrix} 3 \times 3 \times 3, 512, 2 \\ 3 \times 3 \times 3, 512, 2 \end{bmatrix} \times 2$
global average pool	$1 \times 1 \times 1 \times 512$
flatten	embedding of size 512

Table 1: Base 3D ResNet-18 architecture

pared against our proposed model. Our code will be shared to promote reproducibility within the broader community.

3DCNN (baseline): This baseline model is a 4-layer CNN, followed by 2 fully-connected layers, proposed by (Wang et al. 2018). The 3D kernels in the 4 convolutional layers are 1x1x1, 7x7x7, 3x3x3 and 3x3x3, respectively. Except for the first layer, whose stride is 1, all other layers adopt a stride of 2. Furthermore, instead of max pooling on the final feature maps, (Wang et al. 2018) uses global average pooling (He et al. 2016). The resulted feature maps are flattened and fed into a classifier with 2 fully-connected layers, whose output dimensions are 64 and 7, respectively. This model accounts for the temporal dimension of fMRI data by using 1x1x1 convolution (thus treating the temporal dimension as extra channels) to generate a descriptor for every voxel weighted across the time series.

3DResNet (baseline): This baseline model extends 3DCNN by adopting residual connections and bottleneck blocks from ResNet. We augmented the 2D ResNet-18 (He et al. 2016) into its 3D counterpart, referred to as 3D ResNet-18, as shown in Table 1. Like the 3D CNN model, temporal information is pooled by a 1x1x1 conv layer, generating 64 feature maps of the same spatial dimensions (as a single 3D frame). But instead of putting these feature maps through a 4-layer CNN (as in the 3D CNN model), the feature maps are now fed into the 3D ResNet-18 model, which outputs a 512-dimensional spatio-temporal embedding. In turn, this embedding is fed to a classifier, comprising of 2 fully-connected layers, that computes the logits for the task classification. In all of our experiments, we found 3D ResNet-18 to be superior than the 4-layer CNN in extracting spatial information from individual 3D frames so 3D ResNet-18 is used as our base spatial feature extractor $\sigma(\cdot)$ in the rest of the models.

3DResNet-LSTM (baseline): Instead of using a 1x1x1 convolutional layer (which effectively learns a weighting function across frames), this baseline uses a LSTM to model the temporal information in the data. The use of LSTM has been explored in (Mao et al. 2019) (which used 3D CNN to extract spatial features) and (Pominova et al. 2018) (which used a variant of 3D ResNet, with different number of feature maps, that is tailored for epilepsy-depression fMRI data). This baseline model embeds each 3D frame with the base 3D ResNet-18 (cf. Table 1), then uses an LSTM to model the temporal correlation between the embedded frames. The LSTM model has 2 hidden layers, each with 128 hidden units. The hidden states from each timestep are concatenated and passed to the classifier, which shares the same architecture of 2 fully-connected layers as in previous baselines. Dropout (Srivastava et al. 2014) rate of 0.4 was applied to both the LSTM and classifier.

BAnD (ours): We hypothesize that attention is valuable in modeling the temporal dynamics of fMRI data. Our model, called *Brain Attend and Decode* (BAnD) (cf. Figure 1), adapts the Transformer model to the task of fMRI task state decoding. With this self-attention module, we can gain more insights about the temporal dynamics of our 4D data (i.e., temporal sequence of 3D frames) by visualizing the attention of the Transformer across the time series. The Transformer transforms each embedded 3D frame $\mathbf{e}_t = \sigma(\mathbf{x}_t)$ into a latent vector $\mathbf{z}_t$ that is conditioned with information from other embedded frames. To combine these latent vectors (also known as *transformed embeddings*) into a single representation that can be fed into the classifier, it is possible to average these vectors: $\frac{1}{T}\sum_{t=1}^{T}\mathbf{z}_t$, where T is the length of fMRI sequence and $\mathbf{z}_t$ is the transformed embedding generated by the Transformer. This averaging approach is commonly used to derive sentence embeddings from word embeddings (Cer et al. 2018). However, averaging weighs each 3D frame equally, effectively forcing the attention scores to be the same across all frames, thus rendering it impossible to visualize which frames are the most relevant in the task state decoding problem. Instead, we adopt the approach in (Devlin et al. 2018), whereby we insert a shared artificial token ($\mathbf{e}_\star$) to the beginning of each series and train it together with the Transformer. This can be understood as the one "frame" that extracts essential information from the entire time series. By visualizing the attention of that frame on the other frames, this provides insights about which frames are important to the classification problem. With this approach, we retain the ability to visualize the attention of the whole Transformer.

The workflow of BAnD is summarized in Figure 1. Similar to 3DResNet-LSTM, we apply the base 3D ResNet-18 to embed each frame of the data, i.e., $\mathbf{e}_t = \sigma(\mathbf{x}_t)$ for $t = 1, ..., T$. A special pooling token $\mathbf{e}_\star$ is concatenated to this series, i.e., $\{\mathbf{e}_\star, \mathbf{e}_1, ..., \mathbf{e}_T\}$. Positional encoding (Vaswani et al. 2017) is added to each embedding to enable position understanding. The Transformer will then transform these embeddings $\{\mathbf{e}_\star, \mathbf{e}_1, ..., \mathbf{e}_T\}$ into latent vectors $\{\mathbf{z}_\star, \mathbf{z}_1, ..., \mathbf{z}_T\}$. The pooling token $\mathbf{z}_\star$ is fed into a classifier (comprised of 2 fully-connected layers with output dimensions of 512 and the number of classes) to get the logits for task classification. Finally, softmax is applied to get output probabilities for each class.

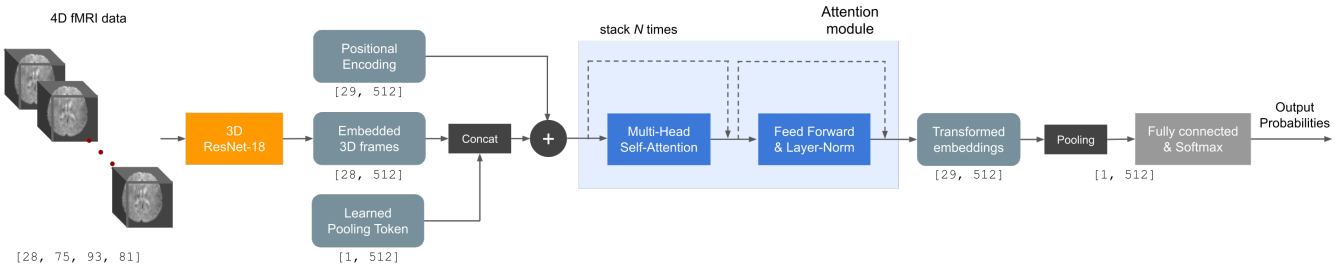

Figure 1: BAnD architecture. Our model has $N = 2$. We show input dimensions at each component for the HCP 7-task dataset.

Through empirical experiments, we optimized the number of attention layers to 2 and attention heads to 8 for the Transformer. Dropout rate of 0.2 was applied to the Transformer and classifier layers.

Environment and Packages

We used PyTorch[1] for our implementation. The Transformer code was adapted from the PyTorch-Transformers repo[2], which was developed for NLP tasks. Our experiments were carried out on an IBM Power8 computing cluster. Each node on this cluster is equipped with 4 Nvidia P100 GPU cards.

For BAnD and 3DResNet-LSTM, because we embedded each 3D frame individually before passing the embeddings to the temporal model, limited GPU memory was an issue. Due to the size of each data instance (i.e., a sequence of 3D frames), we can only fit a batch size of 2 on each GPU card. We found this to cause the models to take a significantly long time to converge. To speed up training, we implemented a distributed training scheme with model parallelization that used 32 (8 computing nodes) GPU cards, which effectively increased the batch size to 64.

Datasets

HCP 7-task

The HCP fMRI dataset includes 7 functional tasks, each under different conditions. These 7 tasks as a whole provide good brain activation coverage (Barch et al. 2013), thus a classifier trained on this dataset would be useful for brain state decoding on a wide range of functional tasks. We used the same data as (Wang et al. 2018) (cf. Table 2), which is a subset of the full HCP fMRI data. Like (Wang et al. 2018), we cropped out empty regions in the raw fMRI data, so the spatial dimensions $[d_x, d_y, d_z]$ are reduced from $[91, 109, 91]$ to $[75, 93, 81]$. The data from (Wang et al. 2018) included 8 extra seconds post task/condition. We omitted these extra post frames (sampled at 0.72 frames per second) and examined only the frames during the actual task/condition. Depending on the task c, our data instance varies in its dimensions $[T_c, d_x, d_y, d_z]$ where $[d_x, d_y, d_z]$ are same as above, but T_c ranges from 16 to 38.

[1]https://pytorch.org/, version 1.2

[2]https://github.com/huggingface/pytorch-transformers

Task - Condition	# Frames	# Instances	Percentage
Emotion - Fear	25	2,895	16.7%
Gambling - Loss	38	1,930	11.1%
Language - Present story	28	3,860	22.2%
Motor - Right hand	16	1,930	11.1%
Relational - Relation	22	2,895	16.7%
Social - Mental	31	2,893	16.6%
WM - 2-back places	38	965	5.6%

Table 2: HCP 7-task dataset summary

Only 965 of the 1,034 subjects performed all 7 tasks in this benchmark. For each task, a subject might have performed more than one run. The total number of 4D data instances in this dataset is 17,368, with class distribution as shown in Table 2. The 17,368 instances were partitioned into train set (70%), validation set (10%) and test set (20%).

Data Processing

It was important to normalize each data instance to have the same number of timesteps. Otherwise, the temporal model would simply learn to count frames to infer the task/condition. Following the data processing scheme in (Wang et al. 2018), we extracted sets of k contiguous frames from each data instance (i.e., each set is $\mathcal{S} = \{\mathbf{x}_r, \mathbf{x}_{r+1}, ..., \mathbf{x}_{r+k-1}\}$ where r is a random index) for training. During validation and testing, only the set corresponding to $r = 0$ (the first k frames) were selected. For data instances with less than k frames, we looped the time series until k frames are achieved, as is commonly done in video recognition (Carreira and Zisserman 2017). In our experiments, $k = 28$. We also experimented with the striding scheme used in (Mao et al. 2019), e.g., if the stride is set to 2, then every other frame is skipped. This striding scheme makes sense for data with many frames, as is the case with the Attention Deficit Hyperactivity Disorder (ADHD) data studied by (Mao et al. 2019), which has an average of 120 frames, while HCP has an average of 28 frames. In our experiments, we set the stride to 1, which equates to no skipping of frames. Besides cropping the empty regions in the 3D frames, we did not do any other spatial cropping, since the input data has already been aligned to the standard MNI152 space (Van Essen et al. 2013).

Transfer learning

We are interested in the transferability of the features learned with BAnD. To this end, we distilled 3 subsets from HCP to evaluate transfer learning under intra-task (same task, different conditions) and inter-task (different tasks) conditions.
HCP 7-task-b set: This dataset was extracted from HCP and has similar characteristics as the HCP 7-task subset that we used to train BAnD. This dataset is used for the intra-task transfer evaluation. The fMRI tasks are the same, but the conditions are different. Instead of the conditions in Table 2, we have: neutral, win, math, right foot, match, random, 2-back body, for the respective tasks. Pre-processing and augmentation scheme remain the same. There are 18,896 data instances in total.
Motor transfer set: To test the transferability of BAnD features in an inter-task setting, BAnD was trained with data instances from the following 6 tasks: Working memory, Gambling, Relational, Social, Language, Emotion (each with the same single condition from the HCP 7-task subset). Then the model was evaluated on the held-out Motor task, under 5 different conditions: right hand, left hand, right foot, left foot and tongue. There are 9,650 data instances in total.
WM transfer set: This dataset is similar to the Motor transfer set, except the Working Memory (WM) task is held out instead of Motor. Like before, BAnD was trained on all tasks except WM, but is tested under the WM tasks with 4 different conditions: 2-back body, 2-back faces, 2-back places, 2-back tools. There are 3,860 data instances in total.

Results and Analysis

Results for each task are reported with mean and standard deviation from 3 different random splits of training, validation and testing data, whenever applicable. We used Adam optimizer (Kingma and Ba 2014) with weight decay of 0.0001. We empirically finetuned the learning rates for each model and used a cosine annealing schedule.
HCP 7-task: BAnD outperforms all other models, as shown by the increasing accuracy values in Figure 3: from 91.4% with 3DCNN, to 94.5% with 3DResNet, to 95.1% with BAnD. We conjecture that this increase in performance stems from the added attention capability to understand complex spatio-temporal dynamics in 4D fMRI data.

As for the 3DResNet-LSTM model, even though we experimented with an extensive hyperparameter sweep of the number of hidden layers $[1, 2, 3]$, the number of hidden units for each layer $[64, 128, 256]$, the directionality (bi- or uni-) of the LSTM model, as well as different dropout rates $[0.2, 0.4, 0.6]$, the model did not converge to a satisfactory validation/test accuracy. With limited computational budget and time, we trained each of these configurations for 24 hours under a distributed environment with 32 GPU cards. Further work is needed to analyze why these LSTM models did not converge under this HCP benchmark. Nonetheless, our BAnD model was able to converge in under 12 hours with the same computational setting. This might be due to the Transformer's advantage of parallelizability and faster convergence, as confirmed by (Vaswani et al. 2017).

Furthermore, as (Popel and Bojar 2018) noted, a bigger batch size (up to a certain threshold) yields better results with the Transformer model. Due to limited GPU memory, BAnD was trained with a batch size of 2 on each GPU card. To increase the batch size, we froze the 3D ResNet-18 layers in the converged BAnD model and trained a new Transformer on top. With this trick, we were able to increase the batch size from 2 to 128, thus deriving at a new model called BAnD++. From Table 3, BAnD++ shows a significant increase in classification accuracy, from 95.1% to 97.2%. We conjecture that the reason is two-fold: the larger batch size helped, but also BAnD is inherently a joint model. The optimization process tries to find a local minimum for an objective function that involves both the spatial and temporal models, which can be two different moving targets. Freezing the spatial model effectively allows the optimizer to to focus only on the self-attention module, thus increasing performance.

3DCNN	0.914 ± 0.0204
3DResNet	0.948 ± 0.011
3DResNet-LSTM	0.534 ± 0.053
3DResNet-TF (ours)	0.951 ± 0.0062
3DResNet-TF++ (ours)	$\mathbf{0.972 \pm 0.0057}$
3DResNet-LSTM++	0.970 ± 0.0037

Table 3: Results for different models on the 7-task on HCP

To evaluate the results qualitatively, we applied t-SNE (Maaten and Hinton 2008) to visualize the final embeddings generated by the 3D ResNet and BAnD++ models. As can be seen in Figure 2, 3DResNet, though quite effective, was not able to disambiguate clearly the data instances belonging to Emotion, Gambling and Social tasks. On the other hand, BAnD++, with the added capability of a Transformer, was able to separate out those instances into separate groups.
Interestingly, even though the joint model 3DResNet-LSTM did not converge to satisfactory classification performance in our experiments, a model with a 3D ResNet-18 spatial model pre-trained as BAnD, with an LSTM temporal head (denote this model as 3DResNet-LSTM++) achieves similar results to BAnD++. This shows that BAnD with the Transformer head instead of an LSTM head not only made it possible for the spatial feature extractor to converge faster but the learned features are also general enough for a new LSTM to learn the temporal patterns of the 4D fMRI data series, and achieves significant performance.

Transfer learning

In this section, we discuss the experimental results on the transferability of BAnD features under the intra-task and inter-task settings, as described above.
Intra-task, HCP 7-task-b set: The goal of this subset is to investigate whether the features learned with BAnD can transfer to a similar dataset. We first froze the spatial feature extractor (i.e., the 3D ResNet-18 layers) in BAnD trained on HCP 7-task dataset, added a new temporal Transformer head (with the same hyperparameters) and trained it on HCP 7-

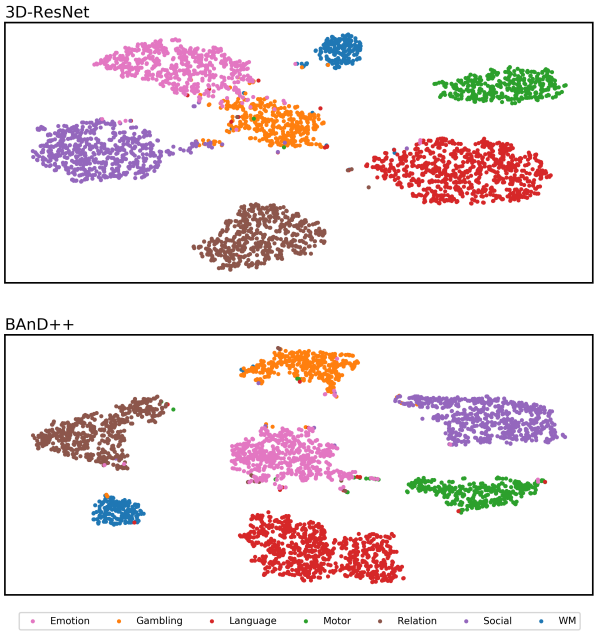

Figure 2: 3DResNet and BAnD++ embeddings t-SNE

task-b dataset, without finetuning the 3D ResNet-18 layers. As can be seen in Table **??**, our model achieved 93.6% accuracy in this setting, which suggests that the spatial features learned with BAnD are highly applicable to similar tasks. Because the spatial embeddings for each 3D frame can be precomputed and saved to disk, this process of only training a new temporal Transformer for a new dataset takes significantly less time than that of training a new joint BAnD model.

Inter-task, Motor transfer: Under this setting, the test tasks are significantly different from the transfer tasks. With the same approach as applied to the HCP 7-task-b, where we froze the 3D ResNet-18 layers in BAnD and trained a new Transformer head, we observed an accuracy of 51.1%. This result suggested that there was room for improvement. Namely, it is clear that further finetuning are needed to learn the new distributions of the transfer tasks. So we further finetuned the 3D ResNet-18 layers to the task of classifying the different Motor conditions. As shown in **??**, we observed a significant increase in classification performance, from 51.1% to 94.1%. Next, we trained a new BAnD model completely from scratch and only on the task of classifying different Motor conditions, denoted as *Motor from scratch* in Figure 3. The model achieved 93.4% classification accuracy, but took significantly more time, while the *Motor with finetuning* model was able to leverage features learned from the tasks it was pre-trained on, and successfully transfer them over to the unseen Motor tasks.

Inter-task, Working Memory transfer: We repeat the experiment above with the held-out WM tasks instead of Motor tasks. We noticed the same patterns as observed in the unseen Motor tasks, in which further finetuning helped our model achieve a significant increase in performance.

7-task-b	0.936 ± 0.012
Motor tasks	0.511 ± 0.027
WM tasks	0.623 ± 0.031
Motor tasks with finetuning	0.941 ± 0.0014
Motor tasks from scratch	0.934 ± 0.0067
WM tasks with finetuning	0.71 ± 0.0043
WM tasks from scratch	0.23 ± 0.018

Table 4: Transfer learning and finetuning results

Notably, for this set of *WM transfer*, the BAnD model that was trained from scratch was far from the accuracy achieved by the model that was pretrained and finetuned, i.e. 23% compared to 71%. It can be due to the relatively smaller size of the *WM transfer* set at 3,860, compared to that of the *Motor transfer set* at 9,650. This shows that the BAnD architecture enables the use of pretraining and finetuning to achieve better classification for smaller datasets.

Analysis

Temporal activation maps: Attention models such as Transformer allows one to examine the attention weights of the model to see which frame is weighted more for a classification result. However, our base BAnD model was trained with 8 attention heads, which makes it hard to discern which set of attention weights is truly important for a classification. Thus, we trained a new BAnD++ with only 1 attention head to make it easier to visualize. To show attention across more frames, we visualize the model's attention weights across $k = 32$ frames. We calculated the attention weights across time for each data instance from the test set that was correctly classified by the model. We then averaged all attention weights in a task to get a representative set of weights. Figure 5 shows the result for the 7 tasks in HCP 7-task benchmark. Interestingly, across different tasks, the 7th frame of a data series seems to have a strong influence on the predictions. This can be due to a delay in the BOLD signal in response to a stimuli (Liao et al. 2002). We include more temporal attention visualizations in the Appendix.

Spatial activation maps: Using Grad-Cam (Selvaraju et al. 2017), we were able to find the set of voxels that were highly activated for a certain class prediction by our BAnD model. We calculated this spatial activation map for each data series, then averaged across data points for a class and picked the 7th frame in each series because our temporal analysis showed that 7th frame was deemed important by the model. We used the nilearn[3] package to project from 3D voxel space to brain statistical maps. Figure 4 shows those for the Motor and Gambling task. Activation maps for other tasks are shown in the Appendix.

To motivate reproducible research in the area of fMRI task state decoding, we plan to release our data processing scripts, codes and pretrained models upon acceptance.

[3]https://nilearn.github.io/

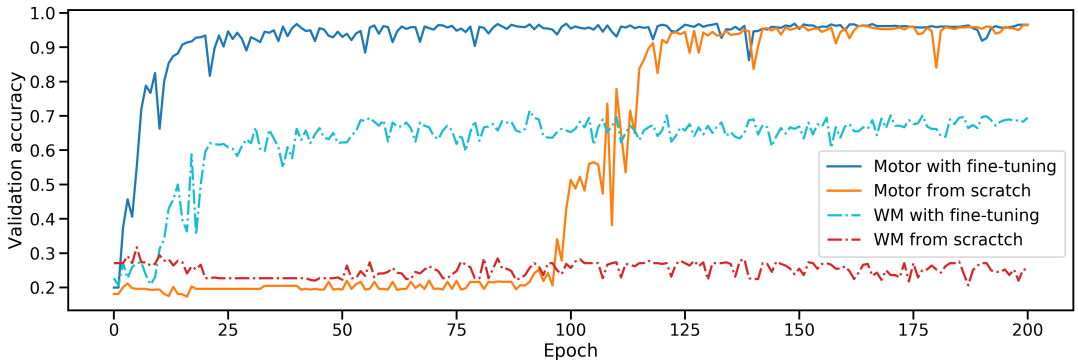

Figure 3: Finetuning vs training from scratch

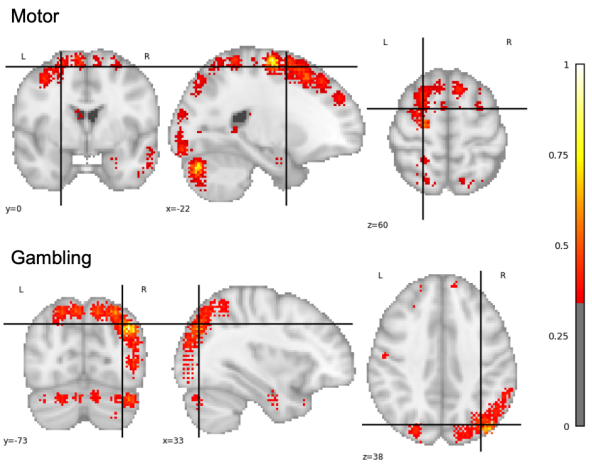

Figure 4: BAnD spatial activation map for Motor (Right hand) and Gambling (Loss) task

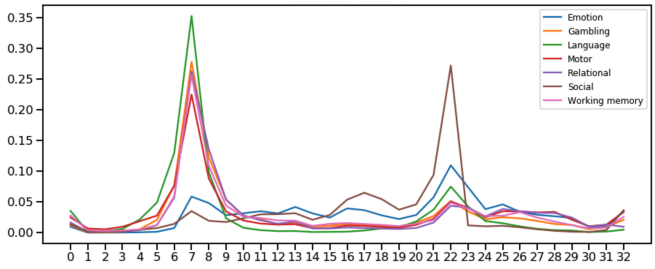

Figure 5: BAnD temporal activation map

Conclusion

In this work, we presented a novel attention-based model for processing 4D fMRI data, and showed that our proposed novel architecture, BAnD, which is based on a multi-headed self-attention module, achieves significant performance gains compared to previous works on a recent 7-task fMRI benchmark from the Human Connectome Project dataset. We further demonstrated transfer learning capability of BAnD's learned features to unseen conditions and tasks and show that BAnD achieves competitive results with fine-tuning. To try to understand what BAnD was attending to for its classifications, we computed both spatial and temporal activation maps, highlighting brain regions and frame important for task decoding. Future work includes transferring BAnD to other fMRI data sets, such as ADHD, or to other modalities of medical imaging.

Acknowledgements

This work was performed under the auspices of the U.S. Department of Energy by Lawrence Livermore National Laboratory under Contract DE-AC52-07NA27344 and was supported by the LLNL LDRD Program under Project No. 19-ERD-009. LLNL-CONF-788817.

References

[Bahdanau, Cho, and Bengio 2014] Bahdanau, D.; Cho, K.; and Bengio, Y. 2014. Neural machine translation by jointly learning to align and translate. *arXiv preprint arXiv:1409.0473*.

[Barch et al. 2013] Barch, D. M.; Burgess, G. C.; Harms, M. P.; Petersen, S. E.; Schlaggar, B. L.; Corbetta, M.; Glasser, M. F.; Curtiss, S.; Dixit, S.; Feldt, C.; Nolan, D.; Bryant, E.; Hartley, T.; Footer, O.; Bjork, J. M.; Poldrack, R.; Smith, S.; Johansen-Berg, H.; Snyder, A. Z.; Van Essen, D. C.; and WU-Minn HCP Consortium. 2013. Function in the human connectome: task-fMRI and individual differences in behavior. *Neuroimage* 80:169–189.

[Carreira and Zisserman 2017] Carreira, J., and Zisserman, A. 2017. Quo vadis, action recognition? a new model and the kinetics dataset. In *proceedings of the IEEE Conference on Computer Vision and Pattern Recognition*, 6299–6308.

[Cer et al. 2018] Cer, D.; Yang, Y.; Kong, S.-y.; Hua, N.; Limtiaco, N.; John, R. S.; Constant, N.; Guajardo-Cespedes, M.; Yuan, S.; Tar, C.; et al. 2018. Universal sentence encoder. *arXiv preprint arXiv:1803.11175*.

[Devlin et al. 2018] Devlin, J.; Chang, M.-W.; Lee, K.; and Toutanova, K. 2018. Bert: Pre-training of deep bidirectional transformers for language understanding. *arXiv preprint arXiv:1810.04805*.

[Girdhar et al. 2018] Girdhar, R.; Carreira, J.; Doersch, C.; and Zisserman, A. 2018. Video action transformer network. *CoRR* abs/1812.02707.

[Glasser et al. 2016] Glasser, M. F.; Smith, S. M.; Marcus, D. S.; Andersson, J. L. R.; Auerbach, E. J.; Behrens, T. E. J.; Coalson, T. S.; Harms, M. P.; Jenkinson, M.; Moeller, S.; Robinson, E. C.; Sotiropoulos, S. N.; Xu, J.; Yacoub, E.; Ugurbil, K.; and Van Essen, D. C. 2016. The human connectome project's neuroimaging approach. *Nat. Neurosci.* 19(9):1175–1187.

[He et al. 2016] He, K.; Zhang, X.; Ren, S.; and Sun, J. 2016. Deep residual learning for image recognition. In *Proceedings of the IEEE conference on computer vision and pattern recognition*, 770–778.

[Hochreiter and Schmidhuber 1997] Hochreiter, S., and Schmidhuber, J. 1997. Long short-term memory. *Neural computation* 9(8):1735–1780.

[Huang et al. 2017] Huang, H.; Hu, X.; Zhao, Y.; Makkie, M.; Dong, Q.; Zhao, S.; Guo, L.; and Liu, T. 2017. Modeling task fmri data via deep convolutional autoencoder. *IEEE transactions on medical imaging* 37(7):1551–1561.

[Kingma and Ba 2014] Kingma, D. P., and Ba, J. 2014. Adam: A method for stochastic optimization. *arXiv preprint arXiv:1412.6980*.

[LeCun et al. 1998] LeCun, Y.; Bottou, L.; Bengio, Y.; Haffner, P.; et al. 1998. Gradient-based learning applied to document recognition. *Proceedings of the IEEE* 86(11):2278–2324.

[Liao et al. 2002] Liao, C. H.; Worsley, K. J.; Poline, J.-B.; Aston, J. A.; Duncan, G. H.; and Evans, A. C. 2002. Estimating the delay of the fmri response. *NeuroImage* 16(3):593–606.

[Litjens et al. 2017] Litjens, G.; Kooi, T.; Bejnordi, B. E.; Setio, A. A. A.; Ciompi, F.; Ghafoorian, M.; Van Der Laak, J. A.; Van Ginneken, B.; and Sánchez, C. I. 2017. A survey on deep learning in medical image analysis. *Medical image analysis* 42:60–88.

[Maaten and Hinton 2008] Maaten, L. v. d., and Hinton, G. 2008. Visualizing data using t-sne. *Journal of machine learning research* 9(Nov):2579–2605.

[Mao et al. 2019] Mao, Z.; Su, Y.; Xu, G.; Wang, X.; Huang, Y.; Yue, W.; Sun, L.; and Xiong, N. 2019. Spatio-temporal deep learning method for adhd fmri classification. *Information Sciences* 499:1–11.

[Naselaris et al. 2011] Naselaris, T.; Kay, K. N.; Nishimoto, S.; and Gallant, J. L. 2011. Encoding and decoding in fmri. *Neuroimage* 56(2):400–410.

[Pereira, Mitchell, and Botvinick 2009] Pereira, F.; Mitchell, T.; and Botvinick, M. 2009. Machine learning classifiers and fmri: a tutorial overview. *Neuroimage* 45(1):S199–S209.

[Pominova et al. 2018] Pominova, M.; Bernstein, A.; Artemov, A.; Burnaev, E.; Sharaev, M.; and Kondratyeva, E. 2018. Voxelwise 3d convolutional and recurrent neural networks for epilepsy and depression diagnostics from structural and functional mri data.

[Popel and Bojar 2018] Popel, M., and Bojar, O. 2018. Training tips for the transformer model. *The Prague Bulletin of Mathematical Linguistics* 110(1):43–70.

[Selvaraju et al. 2017] Selvaraju, R. R.; Cogswell, M.; Das, A.; Vedantam, R.; Parikh, D.; and Batra, D. 2017. Grad-cam: Visual explanations from deep networks via gradient-based localization. In *Proceedings of the IEEE International Conference on Computer Vision*, 618–626.

[Srivastava et al. 2014] Srivastava, N.; Hinton, G.; Krizhevsky, A.; Sutskever, I.; and Salakhutdinov, R. 2014. Dropout: a simple way to prevent neural networks from overfitting. *The journal of machine learning research* 15(1):1929–1958.

[Thomas et al. 2018] Thomas, A. W.; Heekeren, H. R.; Müller, K.; and Samek, W. 2018. Interpretable lstms for whole-brain neuroimaging analyses. *CoRR* abs/1810.09945.

[Van Essen et al. 2013] Van Essen, D. C.; Smith, S. M.; Barch, D. M.; Behrens, T. E. J.; Yacoub, E.; Ugurbil, K.; and WU-Minn HCP Consortium. 2013. The WU-Minn human connectome project: an overview. *Neuroimage* 80:62–79.

[Vaswani et al. 2017] Vaswani, A.; Shazeer, N.; Parmar, N.; Uszkoreit, J.; Jones, L.; Gomez, A. N.; Kaiser, Ł.; and Polosukhin, I. 2017. Attention is all you need. In *Advances in neural information processing systems*, 5998–6008.

[Wang et al. 2018] Wang, X.; Liang, X.; Zhou, Y.; Wang, Y.; Cui, J.; Wang, H.; Li, Y.; Nguchu, B. A.; and Qiu, B. 2018. Task state decoding and mapping of individual four-dimensional fmri time series using deep neural network. *arXiv preprint arXiv:1801.09858*.

[Webb and Kagadis 2003] Webb, A., and Kagadis, G. C. 2003. Introduction to biomedical imaging. *Med. Phys.* 30(8):2267–2267.

[Wen et al. 2018] Wen, D.; Wei, Z.; Zhou, Y.; Li, G.; Zhang, X.; and Han, W. 2018. Deep learning methods to process fmri data and their application in the diagnosis of cognitive impairment: a brief overview and our opinion. *Frontiers in neuroinformatics* 12:23.

[Xu et al. 2015] Xu, K.; Ba, J.; Kiros, R.; Cho, K.; Courville, A.; Salakhudinov, R.; Zemel, R.; and Bengio, Y. 2015. Show, attend and tell: Neural image caption generation with visual attention. In *International conference on machine learning*, 2048–2057.